Formalism for calculation of polymer-solvent-mediated potential

Shiqi Zhou*
Institute of Modern Statistical Mechanics, Hunan University of Technology, Wenhua Road, Zhuzhou City, 412008, People's Republic of China
(Received 27 December 2005; published 20 July 2006)

A simple theoretical approach is proposed for calculation of a solvent-mediated potential (SMP) between two colloid particles immersed in a polymer solvent bath in which the polymer is modeled as a chain with intramolecular degrees of freedom. The present recipe is only concerned with the estimation of the density profile of a polymer site around a single solute colloid particle instead of two solute colloid particles separated by a varying distance as done in existing calculational methods for polymer-SMP. Therefore the present recipe is far simpler for numerical implementation than the existing methods. The resultant predictions for the polymer-SMP and polymer solvent-mediated mean force (polymer-SMMF) are in very good agreement with available simulation data. With the present recipe, change tendencies of the contact value and second virial coefficiency of the SMP as a function of size ratio between the colloid particle and polymer site, the number of sites per chain, and the polymer concentration are investigated in detail. The metastable critical polymer concentration as a function of size ratio and the number of sites per chain is also reported for the first time. To yield the numerical solution of the present recipe at less than 1 min on a personal computer, a rapid and accurate algorithm for the numerical solution of the classical density functional theory is proposed to supply rapid and accurate estimation of the density profile of the polymer site as an input into the present formalism.

DOI: 10.1103/PhysRevE.74.011402 PACS number(s): 82.70.−y

I. INTRODUCTION

Many systems of biological and technological interest can be modeled as colloid particles immersed in a solution of nonadsorbing polymers [1]. Understanding the phase behavior and stability of such dispersions as a function of the polymer concentration, polymer molecular weight, and polymer/colloid size ratio is of primary importance for the development of various industrial applications and probing mechanisms of biological processes. When the size ratio between the colloid particle and the polymer site widens (the colloid particle is larger than the polymer site), a description of the dispersions based on a single component macrofluid approximation becomes more valid [2]. The single component macrofluid approximation needs the polymer-solvent-mediated potential of mean force (polymer-SMP) as an input, therefore detailed understanding, and rapid and accurate obtainment of the polymer-SMP between two colloid particles is of primary importance.

Due to the wide range of particle size ratios and corresponding length scales involved in the problem, simulation studies of the colloid-polymer mixture are notoriously difficult; this only brings out the importance of a theoretical calculation. Although many theoretical works [3] were done on the colloid-polymer system for calculation of the SMP, there do not exist theoretical approaches that are both computationally simple and highly accurate. A straightforward calculational method for polymer-SMP [4] is to solve numerically the polymer-reference interaction site model (PRISM) integral equation theory (IET) [5,6] for a mixture consisting of a solvent polymer and a colloid particle, with the latter component's concentration being zero, to obtain the radial distribution function (RDF) between the two colloid particles, then simply combine the resultant RDF with the Boltzmann relation to obtain the polymer-SMP [4]. Although the PRISM IET, when combined with a unique closure (consistent with field theory), can quantitatively predict colloid structure factors on polymer-colloid suspensions [7], since the case of the polymer-SMP is concerned with an infinite concentration asymmetry and a high size asymmetry, the polymer-SMP from the PRISM IET is not quantitatively accurate, although qualitatively correct [4]. Especially, the predictions from the PRISM IET are very sensitive to the particular closure employed, but there does not exist a general principle for the construction of the closure for the cases of infinite asymmetry in concentration and high asymmetry in size. As long as the accuracy of an adsorption method [8] is concerned, its predictions are even qualitatively incorrect, and it is believed that the qualitative discrepancy of the adsorption method from simulation results is due to the superposition approximation employed. It also is noted that an exact relation [9] can be employed to estimate the SMP from the solvent-mediated excess mean force, which, however, has to be estimated by a three-dimensional (3D) space position $\mathbf{R}$ integration of the solvent conditional density distribution $\rho(\mathbf{R},\mathbf{r})$ equal to the probability of finding the solvent particle at $\mathbf{R}$, given that one solute is at the origin and the other solute is located at $\mathbf{r}$. In the language of density functional theory (DFT), $\rho(\mathbf{R},\mathbf{r})$ is the solvent density distribution under the influence of an external potential due to two solute particles separated by a distance $\mathbf{r}$. Because of the low symmetry of $\rho(\mathbf{R},\mathbf{r})$, its calculation is very intensive computationally. Especially, the calculation of $\rho(\mathbf{R},\mathbf{r})$ has to be done for many different values of $\mathbf{r}$ over which the SMP or SMMF does not disappear. Therefore, the calculational task of the approach is almost comparable to that of a simulation. However, the resultant predictions for both the SMP and SMMF are the most

*Email address: chixiayzsq@yahoo.com

accurate among all existing theoretical approaches, as shown in a recent paper [10], where the SMP between two equal spherical colloid particles immersed in a solution consisting of a freely jointed tangent hard sphere chain is theoretically calculated by a combination of the classical DFT approach for $\rho(\mathbf{R},\mathbf{r})$ and the exact relation [9].

The aim of the present investigation is to propose, in Sec. II a theoretical approach that is comparable in accuracy with the calculationally very extensive method [10], but calculationally the simplest among all existing approaches. With the present approach, we investigate properties of the polymer-SMP, polymer-SMMF, and critical properties of the colloid +polymer system. Considering that the classical DFT approach now becomes a powerful theoretical method for many inhomogeneous phenomena, the present formalism also needs to employ the density profile output of the classical DFT approach as an input for the calculation of the polymer-SMP. However, there does not exist any reported efficient numerical algorithm for the solution of the density profile equation in the classical DFT approach; we also will propose a numerical algorithm for the numerical solution of the classical DFT density profile equation in the Appendix. Finally, we conclude the paper in Sec. III with some discussions.

II. THEORETICAL FORMALISM AND MODEL CALCULATION

The colloid+polymer system under consideration consists of two spherical colloid particles of diameter σ_c at infinitely dilute limit, immersed in a solution of a freely jointed tangent hard sphere chain whose site diameter is denoted by σ_s, the number of the sites per chain is denoted by N_p, and the reduced site number density is denoted by $\rho_{bs}\sigma_s^3=nN_p\sigma_s^3/V$ (here V is the system volume and n is the number of the polymer chain). Following the reasoning in Refs. [3(d),11], the total potential of the mean force (PMF) $\beta W_{cc}(\mathbf{r})$ between two colloid particles at an infinitely dilute limit is a sum of the pure intercolloid pair potential $\beta u_{cc}(\mathbf{r})$ and SMP $\beta u_{ex}(\mathbf{r})$; the total PMF $\beta W_{cc}(\mathbf{r})$ is related to the RDF $g_{cc}(\mathbf{r})$ by

$$\beta W_{cc}(\mathbf{r}) = -\ln[g_{cc}(\mathbf{r})]. \tag{1}$$

In Eq. (1), $\beta=1/k_BT$, where k_B is Boltzmann's constant and T is the absolute temperature (inverse thermal energy or reduced temperature).

According to the Ornstein-Zernike (OZ) IET [12], there exists a closure relation for the colloid-colloid pair,

$$g_{cc}(\mathbf{r}) = \exp\{-\beta u_{cc}(\mathbf{r}) + \gamma_{cc}(\mathbf{r}) + B_{cc}[\gamma_{cc}(\mathbf{r})]\}. \tag{2}$$

Here $\gamma_{cc}(\mathbf{r})$ and B_{cc} are, respectively, the indirect correlation function and the bridge function for the colloid-colloid pair. Then, the SMP $\beta u_{ex}(\mathbf{r})$ is given by

$$\beta u_{ex}(\mathbf{r}) = -\gamma_{cc}(\mathbf{r}) - B_{cc}[\gamma_{cc}(\mathbf{r})]. \tag{3}$$

For multicomponent systems consisting of atomic particles and polymer chains, the structural description is based on a multicomponent PRISM scheme whose starting point is a modified OZ IE [5,6], which takes the connectivity of the chains into account and reads in the Fourier space

$$[I+\hat{H}(q)] = [1-\hat{C}(q)]^{-1}, \tag{4}$$

where I denotes the unit matrix, and $\hat{H}(q)$ and $\hat{C}(q)$ are matrices of functions with

$$\hat{H}_{ij}(q) = \frac{1}{\sqrt{\hat{P}_i(q)\hat{P}_j(q)}}\hat{h}_{ij}(q), \tag{5}$$

$$\hat{C}_{ij}(q) = \sqrt{\hat{P}_i(q)\hat{P}_j(q)}\hat{c}_{ij}(q), \tag{6}$$

where $h_{ij}(r)=g_{ij}(r)-1$ and $c_{ij}(r)$ are, respectively, the total correlation function and second-order direct correlation function (DCF) for a pair of sites belonging to the i and j species. $\hat{P}_i(q)$ is the single chain structure factor of the ith component (equal to 1 for the entire monomeric body). The dimension of all matrices is equal to n, the number of components present in the system. The caret in $\hat{f}_{ij}(q)$ denotes the 3D Fourier transform of $f_{ij}(r)$ normalized with the density factor $\sqrt{\rho_{bi}\rho_{bj}}$, where ρ_{bi} stands for the site number density or particle number density of the species i.

For the present colloid+polymer system, the colloid number density ρ_{bc} is equal to zero, one has the relationship

$$\tilde{\gamma}_{cc}(q) = FT[h_{cc}(\mathbf{r}) - c_{cc}(\mathbf{r})] = \rho_{bs}\tilde{h}_{cs}(q)\tilde{c}_{sc}(q). \tag{7}$$

Here the tilde denotes the 3D Fourier transform. In the real space, Eq. (7) reads

$$\gamma_{cc}(\mathbf{r}) = h_{cc}(\mathbf{r}) - c_{cc}(\mathbf{r}) = \rho_{bs}\int d\mathbf{r}' h_{cs}(\mathbf{r}')c_{sc}(|\mathbf{r}-\mathbf{r}'|). \tag{8}$$

Considering the infinitely dilute limit of the colloid component, the RDF for the colloid-site pair reads $g_{cs}(\mathbf{r})=\rho_{cs}(\mathbf{r})/\rho_{bs}$, with $\rho_{cs}(\mathbf{r})$ being the site density profile around a single colloid particle; $\rho_{cs}(\mathbf{r})$ will be calculated in the present work by a recently proposed polymer DFT approach [13]. According to the definition of the total correlation function, one can calculate the total correlation function $h_{cs}(\mathbf{r})$ by

$$h_{cs}(\mathbf{r}) = g_{cs}(\mathbf{r}) - 1. \tag{9}$$

By taking into account the limit of $\rho_{bc}=0$, one has a relationship for the colloid-site pair,

$$\tilde{h}_{cs}(q) = \hat{P}_s(q)\tilde{c}_{sc}(q) + \hat{P}_s(q)\rho_{bs}\tilde{h}_{cs}(q)\tilde{c}_{ss}(q). \tag{10}$$

Since the colloid particle number density ρ_{bc} is equal to zero in the present colloid+polymer system, the calculation of $\tilde{c}_{ss}(q)$ can be decoupled from the colloidal component. Upon acquiring $\tilde{c}_{ss}(q)$ by the single component PRISM scheme [5,6] and $h_{cs}(\mathbf{r})$ by the DFT approach, one can calculate the $\tilde{c}_{sc}(q)$ by Eq. (10) and $\tilde{\gamma}_{cc}(q)$ by Eq. (7), then one can calculate $\beta u_{ex}(\mathbf{r})$ by Eq. (3) with a specification of B_{cc}. In the following, to make the explanation of the polymer DFT approach [13] clear, the density argument is added to the symbol of the second-order DCF for the site-site pair in

real space and Fourier space, i.e., we write $c_{ss}(r;\rho_{bs})$ and $\tilde{c}_{ss}(q;\rho_{bs})$instead of $c_{ss}(r)$ and $\tilde{c}_{ss}(q)$.

We first summarize the details of the DFT approach [13] for calculation of $\rho_{cs}(\mathbf{r})$, i.e., the site density profile of the freely jointed tangent hard sphere chain under influence of an external field due to a single colloid particle; a detailed derivation can be found in Ref. [13]

$$\rho_{cs}(\mathbf{r}) = \frac{\rho_{bs}}{N_p} F[-\beta\varphi_{ext}(\mathbf{r}),\rho_{cs}(\mathbf{r})] \sum_{i=1}^{N_p} F_i[-\beta\varphi_{ext}(\mathbf{r}),\rho_{cs}(\mathbf{r})] \times F_{N_p+1-i}[-\beta\varphi_{ext}(\mathbf{r}),\rho_{cs}(\mathbf{r})], \tag{11}$$

where

$$F_n[-\beta\varphi_{ext}(\mathbf{r}),\rho_{cs}(\mathbf{r})] = \begin{cases} \int G(\mathbf{r},\mathbf{r}')F[-\beta\varphi_{ext}(\mathbf{r}'),\rho_{cs}(\mathbf{r}')]F_{n-1}[-\beta\varphi_{ext}(\mathbf{r}'),\rho_{cs}(\mathbf{r}')]\,d\mathbf{r}' & n>1, \\ =1 & n=1, \end{cases} \tag{12}$$

for the present freely jointed tangent hard sphere chain, $G(\mathbf{r}_{i+1}-\mathbf{r}_i)=k_c\delta(|\mathbf{r}_{i+1}-\mathbf{r}_i|-\sigma_s)$, constant k_c equals $1/4\pi$ δ is the Dirac function;

$$F[-\beta\varphi_{ext}(\mathbf{r}),\rho_{cs}(\mathbf{r})] = \exp\left(-\beta\varphi_{ext}(\mathbf{r}) - \frac{\delta F_{ex}[\rho_p]}{\delta\rho_{cs}(\mathbf{r})} + \frac{\delta F_{ex}[\rho_p]}{\delta\rho_{cs}(\mathbf{r})}\bigg|_{\rho_p(\mathbf{r})\to\rho_p^b}\right). \tag{13}$$

Here $\rho_p^b=\rho_{bs}/N_p$ is the bulk polymer number density, and $\beta\varphi_{ext}(\mathbf{r})$ is the reduced external potential felt by a polymer site,

$$\beta\varphi_{ext}(r) = \begin{matrix} \propto & r<(\sigma_c+\sigma_s)/2 \\ 0 & r>(\sigma_c+\sigma_s)/2 \end{matrix}. \tag{14}$$

$F_{ex}[\rho_p]$ is the excess Helmholtz free energy of a nonuniform polymer solution, and $\rho_p(\mathbf{R})$ is the molecular density distribution function, and is related with the site density profile $\rho_{cs}(\mathbf{r})$ by

$$\rho_{cs}(\mathbf{r}) = \int \sum_{i=1}^{N_p} \delta(\mathbf{r}-\mathbf{r}_i)\rho_p(\mathbf{R})d\mathbf{R}. \tag{15}$$

$\mathbf{R}=(\mathbf{r}_1,\mathbf{r}_2,\ldots,\mathbf{r}_{N_p})$ denotes the configuration of the polymer chain.

To proceed further, an approximation of $F_{ex}[\rho_p]=F_{ex}[\rho_{cs}]$ is usually made, and thus Eq. (13) reduces to

$$F[-\beta\varphi_{ext}(\mathbf{r}),\rho_{cs}(\mathbf{r})] = \exp\left(-\beta\varphi_{ext}(\mathbf{r}) - \frac{\delta F_{ex}[\rho_{cs}]}{\delta\rho_{cs}(\mathbf{r})} + \frac{\delta F_{ex}[\rho_{cs}]}{\delta\rho_{cs}(\mathbf{r})}\bigg|_{\rho_{cs}(\mathbf{r})\to\rho_{bs}}\right). \tag{16}$$

For the case of $N_p=1$, the present freely jointed tangent hard sphere chain reduces to a hard sphere fluid, and the density profile Eq. (11) reduces to that of the hard sphere fluid under the influence of the external potential Eq. (14) for which an adjustable parameter free version of the LTDFA [14] is very accurate. It was found in Ref. [13] that the parameter free version of the LTDFA [14] can be applied to the present case of $N_p>1$ only if the hard sphere second-order DCF in the parameter free version of the LTDFA [14] is substituted by a scaling $c_{ss}(r;\rho_{bs})$, i.e., $\tau c_{ss}(r;\rho_{bs})$, the value of τ is determined by requiring the resultant scaling second-order DCF $\tau c_{ss}(r;\rho_{bs})$ to have an integrated value $\tau\tilde{c}_{ss}(\mathbf{0};\rho_{bs})$ in agreement with the corresponding value from an equation of state (EOS), i.e.,

$$\kappa = \frac{1}{\rho_{bs}}\left(\frac{\partial\rho_{bs}}{\partial P}\right)_T = \frac{\beta N_p}{\rho_{bs}[1-N_p\rho_{bs}\tau\tilde{c}_{ss}(\mathbf{0};\rho_{bs})]}. \tag{17}$$

Here, P is the bulk pressure of the polymer solution.

To conclude, the term

$$-\frac{\delta F_{ex}[\rho_{cs}]}{\delta\rho_{cs}(\mathbf{r})} + \frac{\delta F_{ex}[\rho_{cs}]}{\delta\rho_{cs}(\mathbf{r})}\bigg|_{\rho_{cs}(\mathbf{r})\to\rho_{bs}}$$

in Eq. (16) can be expressed as

$$\frac{\delta F_{ex}[\rho_{cs}]}{\delta\rho_{cs}(\mathbf{r})} + \frac{\delta F_{ex}[\rho_{cs}]}{\delta\rho_{cs}(\mathbf{r})}\bigg|_{\rho_{cs}(\mathbf{r})\to\rho_{bs}} = \int d\mathbf{r}'[\rho_{cs}(\mathbf{r}')-\rho_{bs}]\tau c_{ss}\left\{|\mathbf{r}-\mathbf{r}'|;\tilde{\rho}_{cs}\left[(\mathbf{r}+\mathbf{r}')/2,\frac{1}{2}\right]\right\}. \tag{18}$$

Here the weighted density

$$\tilde{\rho}_{cs}\left((\mathbf{r}+\mathbf{r}')/2,\frac{1}{2}\right) = \int d\mathbf{r}''\tau c_{ss}[|(\mathbf{r}+\mathbf{r}')/2-\mathbf{r}''|;\rho_{bs}] \times\left[\rho_{bs}+\frac{1}{2}(\rho_{cs}(\mathbf{r}'')-\rho_{bs})\right]/c'_{01s}(\rho_{bs}). \tag{19}$$

Here $c'_{01s}(\rho_{bs})=\int d\mathbf{r}\,\tau c_{ss}(\mathbf{r};\rho_{bs})$.

$c_{ss}(r;\rho_{bs})$ can be obtained by solving numerically the single component PRISM integral equation [6]

$$\tilde{h}(q) = \hat{P}_s(q)\tilde{c}_{ss}(q;\rho_{bs})\hat{P}_s(q) + \rho_{bs}\hat{P}_s(q)\tilde{c}_{ss}(q;\rho_{bs})\tilde{h}(q). \tag{20}$$

Equation (20) can be rearranged into a following form suitable for iteration:

$$\tilde{\gamma}_{ss}(q) = \frac{\tilde{c}_{ss}(q;\rho_{bs})[\hat{P}_s(q)-1] + \rho_{bs}\hat{P}_s(q)\tilde{c}_{ss}^2(q;\rho_{bs})}{1-\rho_{bs}\hat{P}_s(q)\tilde{c}_{ss}(q;\rho_{bs})}. \tag{21}$$

The closure equation for site-site pair is rewritten as

$$c_{ss}(r;\rho_{bs}) = \exp\{-\beta\phi_{ss}(r) + \gamma_{ss}(r) + B_{ss}[\gamma_{ss}(r)]\} - \gamma_{ss}(r) - 1, \tag{22}$$

where $\phi_{ss}(r)$ is the interaction potential between sites. In the present illustrating investigation for the freely jointed tangent hard sphere chain, $\phi(r)$ is of the following form:

$$\phi_{ss}(r) = \propto, \quad r < \sigma_s$$

$$= 0, \quad r > \sigma_s. \tag{23}$$

As was done in Ref. [15], a Percus-Yevick (PY) approximation [12] is employed for the bridge function $B_{ss}(r)$,

$$B_{ss}[\gamma_{ss}(r)] = -\gamma_{ss}(r) + \ln[1+\gamma_{ss}(r)]. \tag{24}$$

The $\hat{P}_s(q)$ appearing in Eqs. (20) and (21) and Eq. (10) can be calculated from an approximate expression for the single chain structure factor determined from the Koyama distribution [16] for a semiflexible hard sphere chain by forcing the energy parameter in the Koyama distribution to be zero.

Regarding the specification of the bridge function $B_{cc}[\gamma_{cc}(\mathbf{r})]$ for the colloid-colloid pair at the infinitely dilute limit, we directly employ the following form suitable for SMP between two colloid particles immersed in a hard sphere solvent bath [17],

$$B_{M\text{-}BPGG}(\gamma) = 0, \quad \gamma < 0$$

$$= [1+s\gamma]^{1/s} - 1 - \gamma, \quad \gamma > 0. \tag{25}$$

Here, s is a function of size ratio between the solvent particle-colloid particle in Ref. [17], where Eq. (25) is employed for calculation of SMP between two colloid particles immersed in a solvent bath consisting of a single component hard sphere fluid, and the resultant SMP is in very satisfactory agreement with the corresponding simulation data. For the present colloid+polymer system, the size ratio should be one between the polymer site and colloid particle, since what is imported into the present formalism is the density profile of the polymer site. The fact that such a choice can reduce the resultant present formalism to the one in Ref. [17], when N_p is equal to 1, also lends support for this choice.

A procedure for the numerical solution of the SMP $\beta u_{ex}(\mathbf{r})$ is given as follows. First, the single component PRISM theory denoted by Eqs. (20)–(23) combined with the PY approximation denoted by Eq. (24) is solved by the algorithm due to Labik *et al.* [18] to obtain $c_{ss}(r;\rho_{bs})$. Then the scaling parameter τ is determined by solving Eq. (17) combined with the EOS proposed in Ref. [19] and denoted therein by Eq. (39). Second, the density profile equation set denoted by Eqs. (11), (12), (14), (16), (18), and (19) are solved numerically to obtain the site density profile $\rho_{cs}(\mathbf{r})$ around a single colloid particle. Third, the total correlation function $h_{cs}(\mathbf{r})$ is obtained by Eq. (9). Then Eq. (10), with $\tilde{c}_{ss}(q)$ being substituted by $\tau\tilde{c}_{ss}(q)$ [$\tau\tilde{c}_{ss}(q)$ instead of $\tilde{c}_{ss}(q)$ is employed in Eq.(10) to be in agreement with the site density profile $\rho_{cs}(\mathbf{r})$, whose acquisition also employs $\tau c_{ss}(r;\rho_{bs})$ instead of $c_{ss}(r;\rho_{bs})$] is employed to obtain $\tilde{c}_{sc}(q)$, and $\tilde{\gamma}_{cc}(q)$ is obtained by Eq. (7). The inverse Fourier transform $\tilde{\gamma}_{cc}(q)$ is used to obtain $\gamma_{cc}(r)$. Fourth, Eq. (3) leads to the desirable SMP $\beta u_{ex}(\mathbf{r})$. In the calculational process, almost all of the calculational time is spent on the calculation of the site density profile $\rho_{cs}(\mathbf{r})$. When the phase behavior of the colloid+polymer system is investigated by importing the $\beta W_{cc}(\mathbf{r}) = \beta u_{cc}(\mathbf{r}) + \beta u_{ex}(\mathbf{r})$ into the single component macrofluid approximation, the $\beta u_{ex}(\mathbf{r})$and therefore the $\rho_{cs}(\mathbf{r})$ have to be computed repeatedly for many bulk state points of the polymer solvent bath. Thus, a fast and accurate numerical algorithm for the solution of the density profile equation set in the DFT approach is very important. In the Appendix, such an algorithm is proposed and employed in the present reported calculation.

The reduced SMMF can be calculated by

$$\sigma_s\beta f_{ex}(r) = -\sigma_s d\beta u_{ex}(r)/dr. \tag{26}$$

In Figs. 1–3, the present theoretical predictions for the polymer-SMP $\beta u_{ex}(\mathbf{r})$ and polymer-SMMF $\sigma_s\beta f_{ex}(\mathbf{r})$ as a function of the colloid-colloid separation for several combinations of chain length N_p, and bulk site number density $\rho_{bs}\sigma_s^3$ at a fixed size ratio $\sigma_c/\sigma_s = 5$, are presented together with the corresponding simulation data [20]. The same comparison is also presented in Figs. 2 and 3 in Ref. [10], where the theoretical predictions are based on the exact relation [9], which, however, has to incur an estimation of the polymer-site conditional density distribution $\rho(\mathbf{R},\mathbf{r})$ as discussed in Sec. I. By comparing the present Figs. 1–3 with Figs. 2 and 3 in Ref. [10], one can conclude that the two theoretical approaches are comparable in accuracy. The calculational task of the present approach is basically equal to a calculation (only one time) of the density profile $\rho_{cs}(\mathbf{r})$ of the site around a single spherically symmetrical colloid particle, since steps III and IV are not associated with the iteration. Step I is common to both the present theory and to that presented in Ref. [10] if the DFT approaches employed in the two theories are the same. However, the theory in Ref. [10] is associated with the estimation of the site density profile around the two spherically symmetrical colloid particles with a different colloid-colloid separation. It is well known that the polymer-site conditional density distribution is two dimensional (2D). The numerical solution of the polymer-site conditional density distribution is much heavier than that of $\rho_{cs}(\mathbf{r})$. To calculate the SMP $\beta u_{ex}(\mathbf{r})$ as a function of the colloid-colloid separation for a fixed combination of bulk parameters by the method in Ref. [10], one has to calculate the polymer-site conditional density distribution for varying $\mathbf{r}$ over which $\beta u_{ex}(\mathbf{r})$ is nonzero. Therefore, compared with the heavy calculational task incurred by the theory in Ref.

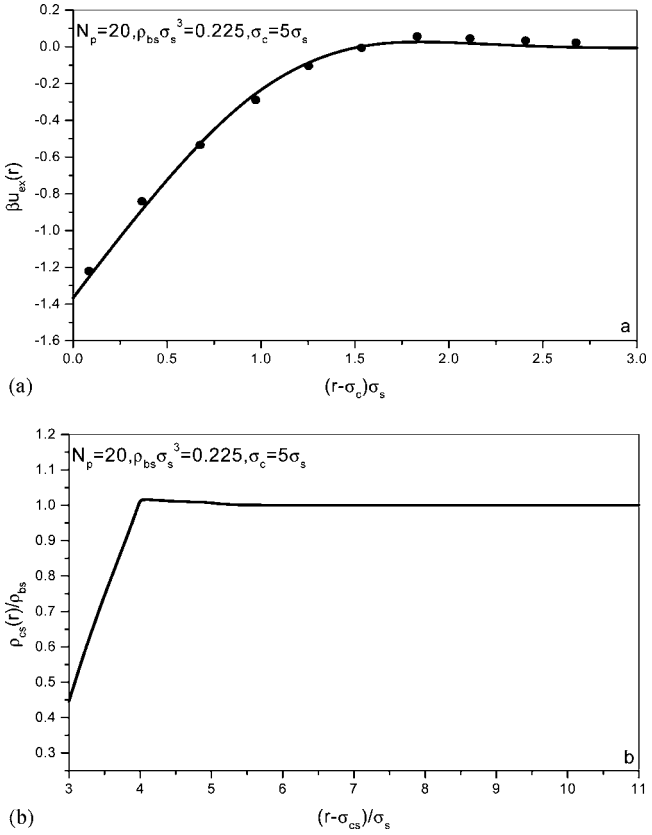

FIG. 1. (a) The SMP $\beta u_{ex}(r)$ vs separation r between two colloid particle. The lines stand for the present theoretical predictions, and symbols are for simulational data [20]. The bulk parameters are shown in the figures. (b) The corresponding reduced site density profile due to the present theoretical calculation.

[10], the calculation time needed by the present approach almost can be neglected.

A fast and accurate estimation of the SMP $\beta u_{ex}(\mathbf{r})$ by the present theoretical approach allows for a theoretical investigation on the phase behavior of the colloid+polymer system on the level of the single component macrofluid approxima-

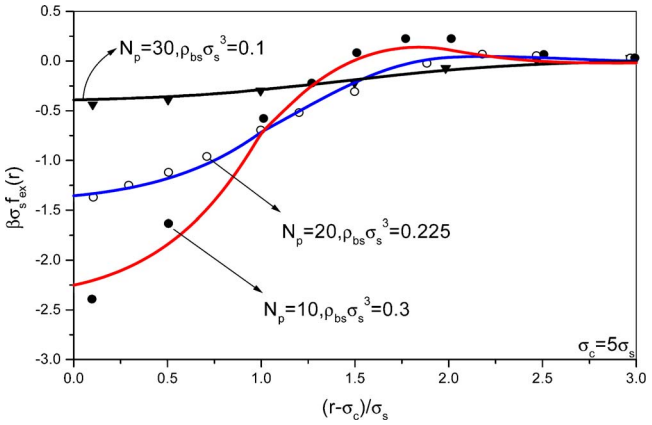

FIG. 2. (Color online) The reduced SMMF $\sigma_s \beta f_{ex}(r)$ vs separation r between two colloid particles. The lines stand for the present theoretical predictions, and symbols are for the simulational data [20]. The bulk parameters are shown in the figures.

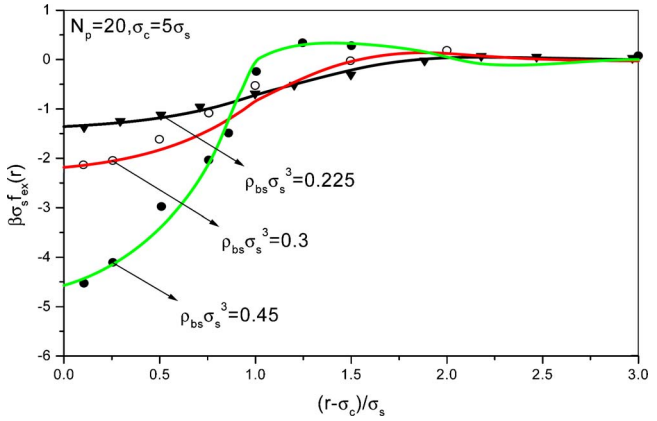

FIG. 3. (Color online) The same as in Fig. 2, but for a different combination of bulk parameters.

tion. Before such an investigation, we first investigate the change tendency of the SMP $\beta u_{ex}(\mathbf{r})$ as the system parameters change.

Figure 4 presents the theoretically predicted $\beta u_{ex}(\mathbf{r})$ for varying $\rho_{bs}\sigma_s^3$ and N_p at a fixed size ratio $\sigma_c/\sigma_s=5$. Compared with the $\beta u_{ex}(\mathbf{r})$ for the colloid+atomic hard sphere fluid system (i.e., $N_p=1$ limit of the present system) investigated in Refs. [17,11], the present amplitude of oscillation of $\beta u_{ex}(r)$ vs r is very weak. Especially when $\rho_{bs}\sigma_s^3$ is very low, the $\beta u_{ex}(r)$ almost monotonously increases to zero. As $\rho_{bs}\sigma_s^3$ increases, $\beta u_{ex}(r)$ becomes more oscillatory, but it is still much weaker than that in the case of the $N_p=1$ limit. As the N_p increases, the oscillation becomes weaker. All of the above observed oscillatory properties can be ascribed to the monotonous behavior of $\rho_{cs}(\mathbf{r})$ at low $\rho_{bs}\sigma_s^3$, as shown in Fig. 1(b), and the weak oscillatory behavior of the $\rho_{cs}(\mathbf{r})$ for increasing $\rho_{bs}\sigma_s^3$, as shown in Fig. 5, and the observation that increasing $\rho_{bs}\sigma_s^3$ has a similar function as displayed by decreasing N_p.

Since the oscillation is weak, the global behavior of the SMP $\beta u_{ex}(r)$ is mainly determined by the contact potential $\beta u_{ex}(\sigma_c)$. Therefore we will investigate in detail the change tendency of the $\beta u_{ex}(\sigma_c)$ as the bulk parameters are changed. In Fig. 6, the influence of σ_c/σ_s and $\rho_{bs}\sigma_s^3$ on $\beta u_{ex}(\sigma_c)$ is presented for a fixed $N_p=15$. Although an increase of $\rho_{bs}\sigma_s^3$ also results in an increase of the site density near the colloid particles, however, the amplitude of the increase is smaller than that in the bulk fluid due to an entropy loss of the polymer chain when situated near the colloid particle. The resulting consequence is a decrease in $\beta u_{ex}(\sigma_c)$ caused by the osmotic pressure difference between the inside region and the outside region of two colloid particles. Figure 6 also shows that $\beta u_{ex}(\sigma_c)$ becomes more attractive when σ_c/σ_s increases. This can be due to two mechanisms. One is that the entropy loss due to the polymer site situated near the colloid particle is strengthened when the colloid particle diameter increases, but this mechanism is not the main one, which should be the increase of the surface area of the colloid particles. When the diameter of the colloid particle is large enough (for example, $\sigma_c/\sigma_s \geq 40$), the entropy loss should be unchanged even if the diameter of the colloid par-

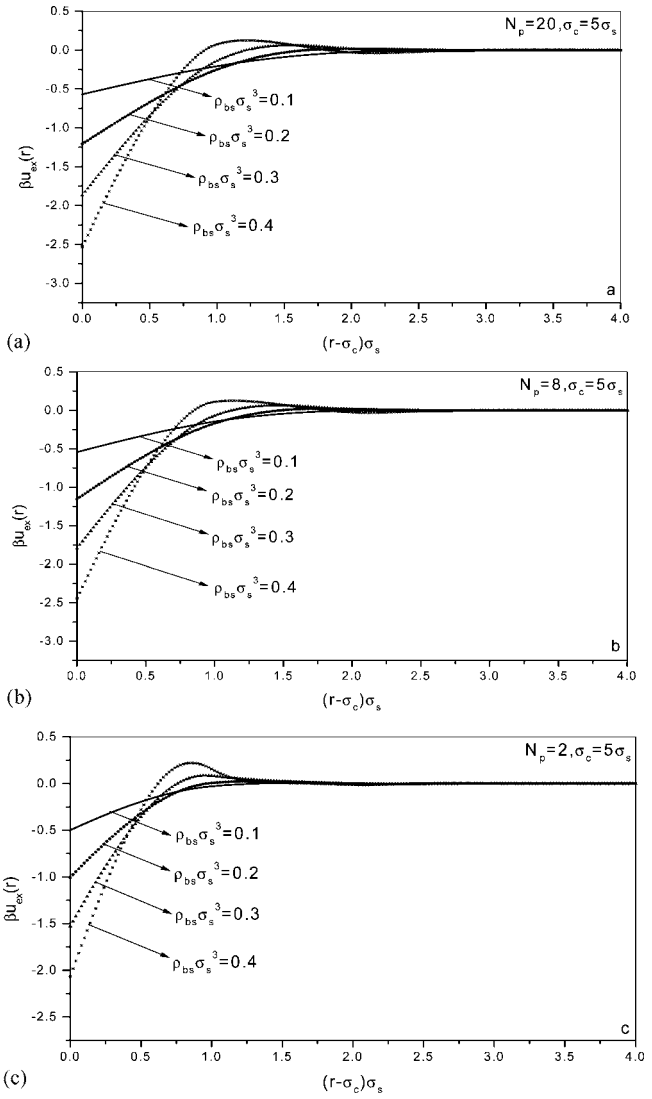

FIG. 4. The theoretical predictions for the SMP $\beta u_{ex}(r)$ vs separation r between two colloid particles. (a), (b), and (c) differ from each other by the parameter combinations as shown in the figures.

ticle increases further, but $\beta u_{ex}(\sigma_c)$ still decreases linearly as σ_c/σ_s increases. Even if the interaction potential energy per unit surface area is unchanged, the total potential energy should increase as the colloid diameter increases.

In Fig. 7(a), the contact SMP $\beta u_{ex}(\sigma_c)$ as a function of the site number N_p per chain is presented for a fixed $\rho_{bs}\sigma_s^3 = 0.35$ and $\sigma_c/\sigma_s = 5$. When the polymer chain is situated near a colloid particle, the freedom degree of a longer chain will be decreased more than that of a shorter polymer chain, therefore the entropy loss is larger for the long chain than for the short chain. This is reflected in Fig. 7(b), where one can conclude that the site number density is lower for the long chain than it is for short chain at a fixed $\rho_{bs}\sigma_s^3$. The resultant consequence is that the contact SMP $\beta u_{ex}(\sigma_c)$ becomes more negative for a long chain than it is for a short chain, as shown in Fig. 7(a).

The second virial coefficient of a fluid is an important quantity for measuring the relative ratio of the repulsion interaction and attraction interaction in a total interparticle po-

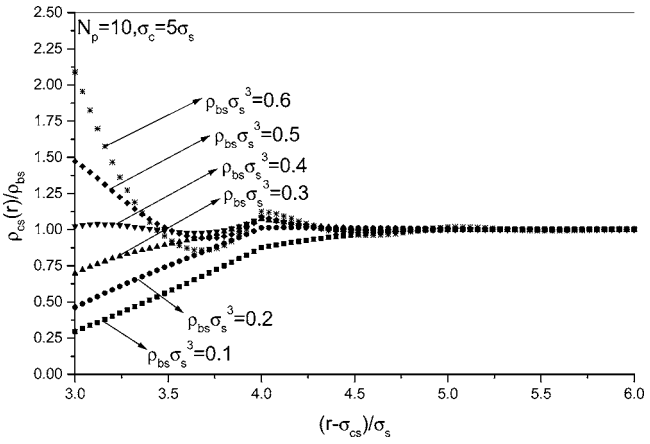

FIG. 5. The reduced site density profile due to the present theoretical calculation for several combinations of bulk parameters.

tential. Recently, it was indicated [21] that, whereas the critical point is very sensitive to the range of interaction, the second virial coefficient has a relatively constant value at the critical temperature. This enables one to predict the critical temperature with fair accuracy only by the second virial coefficient. For the present investigated colloid+polymer system, the bulk $\rho_{bs}\sigma_s^3$ is analogous to the inverse reduced temperature β. Thus, the critical site number density $\rho_{bs}^{cri}\sigma_s^3$ can be simply calculated by the second virial coefficient of the

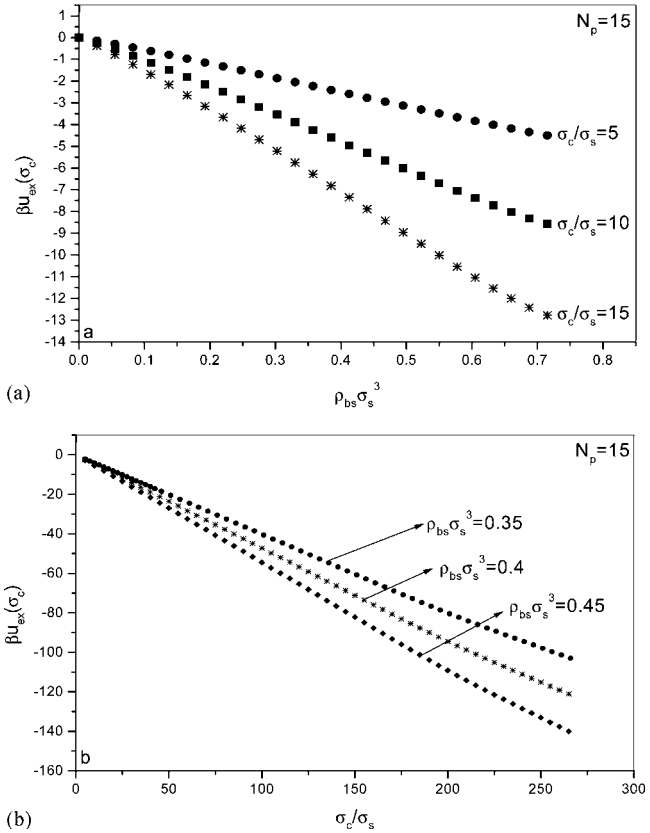

FIG. 6. The contact SMP $\beta u_{ex}(\sigma_c)$ vs (a) $\rho_{bs}\sigma_s^3$ for several size ratios σ_c/σ_s and (b) σ_c/σ_s for several bulk site number densities at fixed $N_p = 15$.

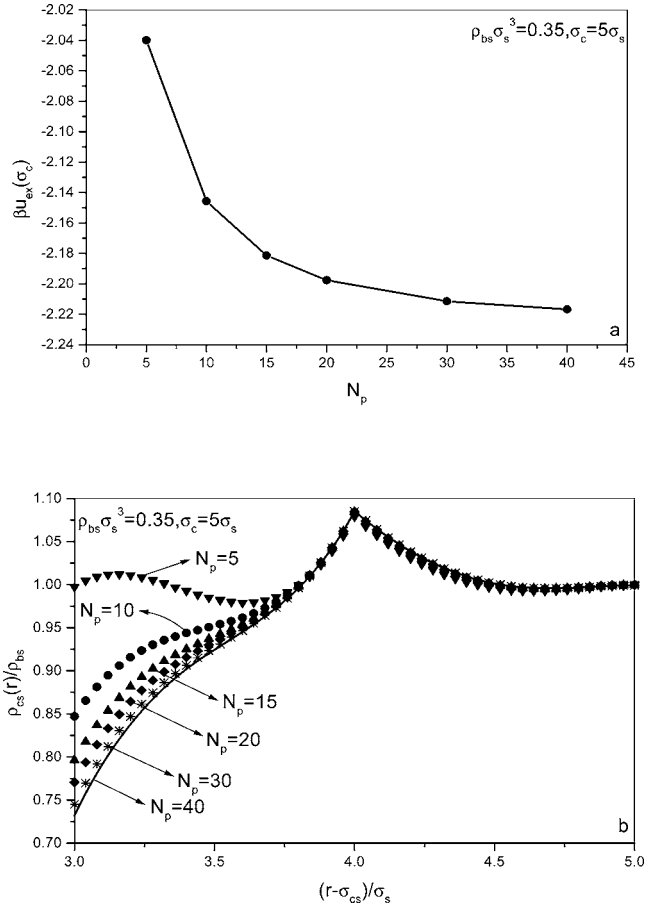

FIG. 7. The contact SMP $\beta u_{ex}(\sigma_c)$ vs N_p for bulk parameter combinations of $\rho_{bs}\sigma_s^3=0.35$ and $\sigma_c/\sigma_s=5$.

colloid+polymer system on the level of the single component macrofluid approximation. It was discovered in Ref. [21] that, when the second virial coefficient B_2 of a fluid, whose potential includes a steep repulsion at a short distance and an attraction at longer distance, satisfies

$$B_2 = -\pi\sigma^3, \tag{27}$$

then the fluid must be close to its critical temperature. Here σ is in all cases taken to be the distance at which the potential crosses zero. For the present system, σ should be σ_c.

To investigate how $\rho_{bs}^{cri}\sigma_s^3$ changes as the bulk parameters change, we first theoretically calculate B_2 for various $\rho_{bs}\sigma_s^3$ and N_p at a fixed $\sigma_c/\sigma_s=5$ to illustrate our aim, and we present the results in Fig. 8,

$$B_2 = 2\pi\int_0^\infty \{1-\exp[-\beta W_{cc}(r)]\}r^2dr. \tag{28}$$

Here

$$\beta W_{cc}(r) = \propto, \qquad r < \sigma_c$$

$$= \beta u_{ex}(r), \quad r > \sigma_c. \tag{29}$$

As expected from the above discussion about the SMP $\beta u_{ex}(r)$, B_2 becomes more negative as N_p and/or $\rho_{bs}\sigma_s^3$ increase. One also observes that the decrease of B_2 will tend to

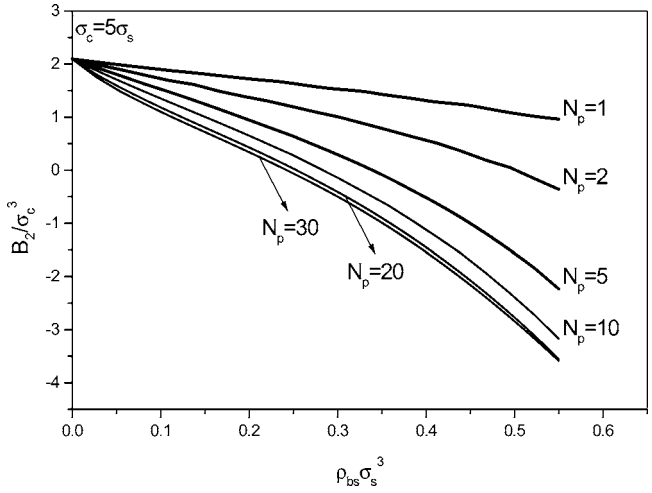

FIG. 8. The reduced second virial coefficient B_2/σ_c^3 vs $\rho_{bs}\sigma_s^3$ for several bulk parameter combinations as shown in the figure.

cease when N_p arrives at a high value, for example, 20. This is due to the fact that the entropy loss tends to a saturation value when N_p arrives at a high value. The decrease of B_2 tends to accelerate as $\rho_{bs}\sigma_s^3$ increases.

In Fig. 9, $\rho_{bs}^{cri}\sigma_s^3$ as a function of N_p and σ_c/σ_s is presented. The specification of $\rho_{bs}^{cri}\sigma_s^3$ is based on the empirical criterion Eq. (27). It was discovered that increasing N_p and/or σ_c/σ_s tends to decrease $\rho_{bs}^{cri}\sigma_s^3$. When σ_c/σ_s increases to a large value, for example, $\sigma_c/\sigma_s=16$ or 20, the decreasing tendency of $\rho_{bs}^{cri}\sigma_s^3$ will become not so obvious as in the case when σ_c/σ_s is small. Although the contact SMP $\beta u_{ex}(\sigma_c)$ will become more negative when σ_c/σ_s increases, the interaction range will become shorter at the same time. From Eq. (28), one knows that the integrand is proportional to r^2, but is related to $\beta u_{ex}(\sigma_c)$ by an exponent function. Therefore, $\rho_{bs}^{cri}\sigma_s^3$ will tend to a saturation value when σ_c/σ_s arrives at a large value.

III. SUMMARY

A new methodology is proposed for calculation of the SMP $\beta u_{ex}(r)$ between two large solute particles immersed in

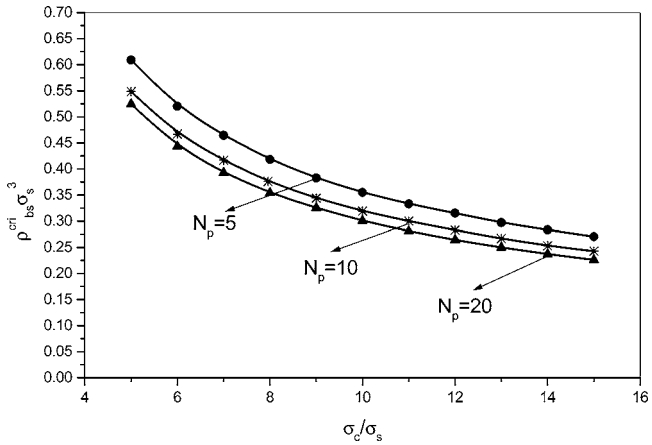

FIG. 9. The critical $\rho_{bs}^{cri}\sigma_s^3$ vs σ_c/σ_s for several different N_p.

a polymer solvent bath. Since the present method is based on the modified OZ IE, which, in principle, can be applied to molecules of any shape and systems with any number of components in the solvent bath, therefore the extension of the present methodology to a solute particle of arbitrary shape and a solvent bath of any components (atomic and/or polymeric component or their mixture) is straightforward.

The present methodology consists of decoupling the PRISM IE for a multicomponent mixture at the infinitely dilute limit of the solute species and applying the equivalence between the RDF $g_{cs}(\mathbf{r})$ for a solvent-solute pair of zero solute density limit and the reduced density profile $\rho_{cs}(\mathbf{r})/\rho_{bs}$ of a solvent around a single solute, i.e., $g_{cs}(\mathbf{r})=\rho_{cs}(\mathbf{r})/\rho_{bs}$. Although the decoupling of the OZ IE and PRISM IE for a multicomponent mixture at the infinitely dilute limit of the solute species is a well-known fact, to the knowledge of the present author, previously the decoupling of the OZ IE is only employed to simplify the solution of the many component OZ IE to calculate the SMP between two walls immersed in a solvent bath of atomic fluid [22]. However, for the case of two walls, the SMP can be tackled easily by the DFT approach by making use of the single coordinate over which the density variation occurs. In Ref. [22], the equivalence of $g_{cs}(\mathbf{r})=\rho_{cs}(\mathbf{r})/\rho_{bs}$ is not made use of. Instead, one is confronted with the problem of choosing or devising appropriate bridge function approximations for both the solvent-solute pair and the solute-solute pair. In Ref. [22], because of the absence of appropriate bridge function approximations, the HNC approximation is employed for both the solvent-solute pair and the solute-solute pair. Therefore the theoretical calculation in Ref. [22] is only qualitative. Reference [23] also makes use of decoupling the PRISM OZ IE for a two-component mixture, but to investigate the adsorption of the chain fluid in slitlike pores, in this work, the equivalence $g_{cs}(\mathbf{r})=\rho_{cs}(\mathbf{r})/\rho_{bs}$ also is not employed. Therefore Ref. [23] also does not get around the problem of choosing or devising an appropriate bridge function approximation for the solvent-solute pair. The combination of the decoupling with the equivalence$g_{cs}(\mathbf{r})=\rho_{cs}(\mathbf{r})/\rho_{bs}$ is proposed and applied for the first time in the present paper for a polymer solvent bath, and in several recent papers [24,17,3,11], also due to the present author for a hard sphere and a Lennard-Jones solvent bath to predict the SMP between two large solute particles. In the present paper and in Refs. [24,17,3,11], the equivalence $g_{cs}(\mathbf{r})=\rho_{cs}(\mathbf{r})/\rho_{bs}$ is made use of and the DFT approach is employed for calculation of $\rho_{cs}(\mathbf{r})$. Therefore the present paper and Refs. [24,17,3,11] get around the problem of choosing or devising an appropriate bridge function approximation for the solvent-solute pair by employing the DFT approach for calculation of $\rho_{cs}(\mathbf{r})$. Nowadays, the DFT approach is highly developed and accurate, while the bridge function approximation for the case of high asymmetry of concentration and size is still at the very rudimentary stage. Therefore, the combination of the equivalence $g_{cs}(\mathbf{r})=\rho_{cs}(\mathbf{r})/\rho_{bs}$ with the DFT approach, as done in the present paper and in Refs. [24,17,3,11], yet can be regarded as a wise method for improving accuracy. For the case of two particles at a certain separation, the SMP cannot be tackled easily by the DFT approach [10] without incurring an intensive computational task since there is not a single coordinate (as is the case for one colloid or for two planar surfaces) over which the density variation occurs. As discussed in Introduction and in the following, the computational task is very intensive for the case of two particles, and this only brings out the importance of thepresent methodology.

Improvement in the numerical efficiency of the present approach over the one discussed in Ref. [10] can be estimated quantitatively as follows. Assuming that $\beta u_{ex}(\mathbf{r})$ and $\sigma_s\beta f_{ex}(\mathbf{r})$ disappear after the particle separation r goes beyond a limit value $r_{2\,\max}\sigma_s$, then one has to calculate $\beta u_{ex}(\mathbf{r})$ and $\sigma_s\beta f_{ex}(\mathbf{r})$ on a grid of equal distance Δr_2 from σ_c to $r_{2\,\max}\sigma_s$. In Ref. [10], each calculation for $\beta u_{ex}(\mathbf{r})$ and/or $\sigma_s\beta f_{ex}(\mathbf{r})$ with r between σ_c and $r_{2\,\max}\sigma_s$ involves one estimation of $\rho(\mathbf{R},\mathbf{r})$. Then $\rho(\mathbf{R},\mathbf{r})$ has to be calculated, but on a 2D grid. Assuming that the grid number for calculation of $\rho_{cs}(\mathbf{r})$ is N_{1iter}, then, on average, the grid number N_{2iter} for the calculation of $\rho(\mathbf{R},\mathbf{r})$ should be $N_{2iter}=1.2N_{1iter}0.5\pi/0.04$ [assuming the numerical calculation is carried out in a spherical coordinate system and the grid distance for the angle integration is 0.04; the coefficient 1.2 takes into account that the nonconstant region of $\rho(\mathbf{R},\mathbf{r})$ is larger than that of $\rho_{cs}(\mathbf{r})$, and coefficient 0.5 takes into account the symmetry]. Then, for a calculation of $\beta u_{ex}(\mathbf{r})$ and/or $\sigma_s\beta f_{ex}(\mathbf{r})$ from σ_c to $r_{2\,\max}\sigma_s$ by the approach discussed in Ref. [10], the total number N_{2total} of the calculation for the right-hand side of Eq. (11) should be $(r_{2\,\max}\sigma_s-\sigma_c)/\Delta r_2$ times N_{2iter}. Therefore the present approach is faster than that given in Ref. [10] by a multiple $N_{2iter}(r_{2\,\max}\sigma_s-\sigma_c)/\Delta r_2 N_{1iter}$. From Figs. 1–3, $(r_{2\,\max}\sigma_s-\sigma_c)$ is at least $6\sigma_s$; if, $\Delta r_2=0.04\sigma_s$ then the multiplet is 7065. Such an estimation has not taken into account an unfavorable factor of the approach given in Ref. [10] that the algorithm's convergence ratio for the 2D grid is slower than that for the 1D grid. However, the most serious problem for the approach given in Ref. [10] appears when the solvent is situated both near the critical point state or at the critical point. At or near the critical point, the long range density fluctuation makes the SMP and SMMF exponentially long ranged with the solvent bath bulk correlation length. As a conservative estimation, if $(r_{2\,\max}\sigma_s-\sigma_c)$ is estimated to be $100\sigma_s$, then the multiple will be 117 750. Therefore one can conclude that the present improvement in numerical efficiency over the approach in Ref. [10] is not marginal, but tremendous. The approach in Ref. [10] is practically not applicable to the calculation of the SMP due to the solvent bath being situated at and/or near the critical point, but the present methodology is applicable to the critical solvent bath as well as the solvent bath far from the critical point. The only input of the present methodology is the solvent density profile around a single solute particle. Therefore the calculational task of the present method is not heavier than that of obtaining the solvent density profile with the spherical symmetry. From the point of calculational simplicity and calculational time needed, the present method is the simplest of the existing methods for the SMP. The algorithm proposed in the Appendix supplies a rapid and accurate iteration procedure for obtaining the density profile by DFT approach. Therefore

the present formalism for the SMP in combination with the present algorithm enables the calculation of the SMP to be completed in less than 1 min on a personal computer. This will greatly quicken the calculation of the phase behavior of complex fluids.

The present calculation also establishes the validity of a well-known Asakura-Oosawa (AO) depletion potential [25] for the colloid+polymer system at certain conditions. The AO depletion potential originates from an assumption that the polymers are described as noninteracting spherical particles, which, however, interact with colloidal particles through a hard sphere repulsion. The assumption of spherical particles instead of a polymer long chain underestimates the entropy loss associated with the shift of the polymer chain toward the surface of the colloid particles, therefore overestimating the density profile between the regions of the two colloid particles. However, the assumption of noninteraction instead of the hard sphere repulsion between sites will underestimate the density profile between the regions of the two colloid particles, since the noninteracting spherical particles will tend to move out of the regions between the two colloid particles to avoid the repulsion interaction between the colloid particle and the polymer spherical particle (the polymer spherical particles have no interaction with each other in bulk as assumed in the AO theory). Cancellation of these two effects leads to the observation that the simple AO depletion potential contains the essential features of the SMP $\beta u_{ex}(r)$. It also should be pointed out that the cancellation is not complete when N_p and $\rho_{bs}\sigma_s^3$ become small enough and large enough, respectively. Low N_p and/or high $\rho_{bs}\sigma_s^3$ induce obviously oscillatory $\beta u_{ex}(r)$ while the AO depletion potential still monotonously tends to zero.

In nanoparticle systems, the diameter of the nanoparticle is usually at least one order larger than that of other particles in the system. Therefore, a very good description of the structure and thermodynamic properties of the nanoparticle systems can be given by the single component macrofluid approximation in which the nanoparticles interact with each other through the potential of the mean force mediated by the small-size components. The strong size dependence of the contact SMP $\beta u_{ex}(\sigma_c)$ displayed in Fig. 6 certainly has close relevance with the strong size dependence of various nanoparticle properties, such as size-dependent optical, electronic, and magnetic properties that could be useful for a variety of technologies including coating, catalysis, memory, and sensor application [26]. From the view of mapping the nonhard sphere fluid onto a hard sphere fluid with an effective hard sphere diameter, the strong size dependence of the contact SMP $\beta u_{ex}(\sigma_c)$ will also lead to a strong size dependence of the effective hard sphere diameter, and therefore will lead to a strong size dependence of the solid-liquid transition point. This also has close relevance with the size dependence precipitation separation and enables one to prepare nanocrystals with a narrow size distribution.

As pointed out in Ref. [2], the single component macrofluid approximation becomes valid when the size ratio between the solute and solvent particles increases beyond 5. Although Eq. (27) is *ad hoc*, its validity is surely checked by many various model potentials [21]. Therefore one can expect that the finding displayed in Fig. 9 is at least qualitatively correct. For example, Fig. 9 indicates that $\rho_{bs}^{cri}\sigma_s^3$ decreases when σ_c/σ_s increases for three investigated numerical values of N_p. From Fig. 9 one can derive out that for the $N_p=1$ limit of the present system (i.e., the asymmetry binary hard sphere mixture), $\rho_{bs}^{cri}\sigma_s^3$ also will decrease when $\sigma_c\sigma_s$ increases. In fact, Ref. [27] also surely reports the above-mentioned tendency by computer simulation.

Although the gas-liquid coexistence is theoretically predicted, depending on the size ratio σ_c/σ_s, they can be stable or metastable. Recent theoretical [28] and simulational investigations [29] indicate that when the range of attraction is below 20% of the range of the repulsion, the system has no stable liquid phase—just one fluid and one solid phase—and the gas-liquid coexistence curve is metastable with respect to the gas-solid coexistence curve. However, in a supercooled region [30], the rapidly increasing viscosity of the liquid may enable the metastable gas-liquid coexistence to materialize.

ACKNOWLEDGMENTS

This project is supported by the National Natural Science Foundation of China (Grant No. 20546004).

APPENDIX: A NEW NUMERICAL ALGORITHM

Calculation of a self-consistent solution is an ubiquitous problem in the fields of computational physics and chemistry. The classical DFT approach has now evolved into a powerful theoretical tool for investigations on the structure and thermodynamic properties of inhomogeneous fluids. However, there does not exist a rapid and accurate algorithm for the numerical solution of the density profile equation in the classical DFT approach reported. This hinders the widespread application of the classical DFT approach as a routine tool.

A common strategy to obtain a self-consistent solution is by iterative calculations. A traditional iterative procedure is the Picard iteration method [31], which, however, results in poor convergence behavior: either slow convergence even with a good initial guess or divergence overall. The divergence of the Picard method [31] can be cured by Broyles' mixing procedure [32], if a good initial estimate is available, but the convergence is still generally slow especially when the bulk density is high. In the present investigation, we apply an inverse Broyden method to the iteration solution of the density profile equation set denoted by Eqs. (11), (12), (14), (16), (18), and (19).

We solve the density profile equation set on a grid of equal distance Δr from $r=(\sigma_c+\sigma_s)/2$ to $r=(\sigma_c+\sigma_s)/2+7\sigma_s$,

$$\rho_{cs}^{i}((\sigma_c+\sigma_s)/2+(i-1)\Delta r), \quad i=1,2,\ldots,N, \tag{A1}$$

$$\rho_{cs}(\mathbf{r})=0, \quad r<(\sigma_c+\sigma_s)/2$$

$$=\rho_{bs}, \quad r>(\sigma_c+\sigma_s)/2+7\sigma_s. \tag{A2}$$

The 3D integral $\int d\mathbf{r}''\tau c_{ss}[|(\mathbf{r}+\mathbf{r}')/2-\mathbf{r}''|;\rho_{bs}]\{\rho_{bs}+\frac{1}{2}[\rho_{cs}(\mathbf{r}'')-\rho_{bs}]\}/c_{01s}'(\rho_{bs})$ in Eq. (19) can be reduced to a 2D integral,

$$2\pi\int_0^{r'} dr'' \int_0^{\pi} d\theta r''^2 \sin\theta \tau c_{ss}(r'';\rho_{bs})\left[\rho_{bs}+\frac{1}{2}(\rho_{cs}\{\sqrt{(r''\sin\theta)^2+[r''\cos\theta+|(\mathbf{r}+\mathbf{r}')/2|]^2}\}-\rho_{bs})\right] \Big/ c_{01s}'(\rho_{bs}).$$

The integral on radial distance r'' is done by a simple trapezoidal rule [33], while the angle integral is done by a Gaussian method [33]. Under the PY approximation for the freely jointed tangent hard sphere chain, $r'=\sigma_s$. It should be noted that the expression $\rho_{bs}+\frac{1}{2}(\rho_{cs}\{\sqrt{(r''\sin\theta)^2+[r''\cos\theta+|(\mathbf{r}+\mathbf{r}')/2|]^2}\}-\rho_{bs})$ in the integrand is noncontinuous as a function of radial distance r'', therefore, the angle integral should be separated into several regions in which the function is continuous. The integral $\int d\mathbf{r}'(\rho_{cs}(\mathbf{r}')-\rho_{bs})\tau c_{ss}\{|\mathbf{r}-\mathbf{r}'|;\tilde{\rho}_{cs}[(\mathbf{r}+\mathbf{r}')/2,\frac{1}{2}]\}$ in Eq. (18) can be treated similarly, but one first has to calculate the $\tilde{\rho}_{cs}(r,\frac{1}{2})$ from $r=\max[(\sigma_c+\sigma_s)/2-0.5\sigma_s,0]$ to $r=(\sigma_c+\sigma_s)/2+7.5\sigma_s$. Similar to the treatment of the density profile $\rho_{cs}(r)$, one also can only calculate the $\tilde{\rho}_{cs}(r,\frac{1}{2})$ on a grid of equal distance Δr from $r=\max[(\sigma_c+\sigma_s)/2-0.5\sigma_s,0]$ to $r=(\sigma_c+\sigma_s)/2+7.5\sigma_s$, i.e.,

$$\tilde{\rho}_{cs}{}^{j}\{\max[(\sigma_c+\sigma_s)/2-0.5\sigma_s,0]+(j-1)\Delta r\},$$

$$j=1,2,\ldots,N'.$$

The numerical value of $\rho_{cs}(r)$ and $\tilde{\rho}_{cs}(r,\frac{1}{2})$ on the space between grid points can be obtained by interpolation.

Based on the above analysis, one can write the density profile Eq. (11) into a nonlinear equation system with N unknowns,

$$\rho_{cs}^{i}=f\{(\sigma_c+\sigma_s)/2+(i-1)\Delta r;[\rho_{cs}^{1},\rho_{cs}^{2},\ldots,\rho_{cs}^{N}]\}$$

$$i=1,2,\ldots,N. \tag{A3}$$

Here f denotes the functional relationship of Eq. (11).

The algorithm formulas of the inverse Broyden method [34] can be summarized as follows:

$$\mathbf{x}^{k+1}=\mathbf{x}^{k}-\mathbf{H}_k\mathbf{F}(\mathbf{x}^{k}),$$

$$\mathbf{H}_{k+1}=\mathbf{H}_k+\alpha(\mathbf{s}^{k}-\mathbf{H}_k\mathbf{y}^{k})\frac{(\mathbf{s}^{k}-\mathbf{H}_k\mathbf{y}^{k})^{T}}{(\mathbf{s}^{k}-\mathbf{H}_k\mathbf{y}^{k})^{T}\mathbf{y}^{k}},$$

$$k=0,1,\ldots, \tag{A4}$$

where k denotes the kth iteration, $\mathbf{s}^{k}=\mathbf{x}^{k+1}-\mathbf{x}^{k}$, $\mathbf{y}^{k}=\mathbf{F}(\mathbf{x}^{k+1})-\mathbf{F}(\mathbf{x}^{k})$, $\mathbf{H}$ is a $N\times N$ iterative matrix, and $\mathbf{x}$ is a $N\times 1$ matrix given by

$$\mathbf{x}=\begin{bmatrix}\rho_{cs}^{1}\\ \rho_{cs}^{2}\\ \vdots\\ \rho_{cs}^{N}\end{bmatrix}. \tag{A5}$$

$\mathbf{F}$ is a $N\times 1$ matrix given by

$$\mathbf{F}(\mathbf{x})=\begin{bmatrix}\rho_{cs}^{1}-f\{(\sigma_c+\sigma_s)/2+(1-1)\Delta r;[\rho_{cs}^{1},\rho_{cs}^{2},\ldots,\rho_{cs}^{N}]\}\\ \rho_{cs}^{2}-f\{(\sigma_c+\sigma_s)/2+(2-1)\Delta r;[\rho_{cs}^{1},\rho_{cs}^{2},\ldots,\rho_{cs}^{N}]\}\\ \vdots\\ \rho_{cs}^{N}-f((\sigma_c+\sigma_s)/2+(N-1)\Delta r;[\rho_{cs}^{1},\rho_{cs}^{2},\ldots,\rho_{cs}^{N}])\end{bmatrix}. \tag{A6}$$

When $Residual=\mathbf{F}^{T}(\mathbf{x}^{k})\mathbf{F}(\mathbf{x}^{k})\le\epsilon$ (ϵ is the absolute error, usually 10^{-5} or 10^{-9}), $\mathbf{x}^{k}$ is the true solution. To initiate the iteration process of the inverse Broyden method, one has to input $\mathbf{x}^{0}$ and $\mathbf{H}_0$. In the original inverse Broyden method, coefficient α is equal to 1. The present calculation indicates that lowering the α to a lower value, for example, 0.8, can quicken convergence.

Throughout the presented calculations, $\Delta r=0.04\sigma_s$, therefore $N=7\sigma_s/\Delta r+1=176$, $N'=8\sigma_s/\Delta r+1=201$.

For the case of low bulk site number density $\rho_{bs}\sigma_s^3$, for example, $\rho_{bs}\sigma_s^3\le 0.4$, the initial values of $\mathbf{x}$ and $\mathbf{H}$ are set to be $\mathbf{x}^{0T}=[\rho_{bs},\rho_{bs},\ldots,\rho_{bs}]$ and $\mathbf{H}_0=$unit matrix. α can be set to be 1. After 5–7 iterations, the true solution with $\epsilon=10^{-9}$ can be found. When $\rho_b\sigma^3>0.4$, the iteration process, with $\mathbf{x}^{0T}=[\rho_{bs},\rho_{bs},\ldots,\rho_{bs}]$ and $\mathbf{H}_0=$unit matrix, diverges. One has to employ an approximate solution and iteration matrix of the lower bulk density as the input for the case of higher bulk density, and at the same time, lower the value of relaxation factor α, for example, set $\alpha=0.8$. The total iteration times are not beyond 40. For the traditional Broyles' mixing procedure,the iteration times needed to arrive at the true solution with $\epsilon=10^{-9}$ are usually high—up to 500 for case oflow $\rho_{bs}\sigma_s^3$—for example, $\rho_{bs}\sigma_s^3\le 0.42$ with the initial value of $\mathbf{x}^{0T}=[\rho_{bs},\rho_{bs},\ldots,\rho_{bs}]$. For the case of higher $\rho_{bs}\sigma_s^3$, the needed iteration number is high—up to 1000 or 2000 or more. What is more, for the case of higher $\rho_{bs}\sigma_s^3$, the true solution with $\epsilon=10^{-9}$ will never be arrived at. Only the approximate solution with $\epsilon=10^{-3}$ can be found. This obviously cannot satisfy the requirement of higher accuracy exerted by, for example, the present investigation, in which the true solution of the density profile $\rho_{cs}(\mathbf{r})$ is only an input for the next computation.

[1] R. Tuinier, J. Rieger, and C. G. de Kruif, Adv. Colloid Interface Sci. **103**, 1 (2003); R. L. C. Vink and M. Schmidt, Phys. Rev. E **71**, 051406 (2005); D. Frydel and S. A. Rice, *ibid.* **71**, 041402 (2005); K. Jagannathan, G. Reddy, and A. Yethiraj, J. Phys. Chem. B **109**, 6764 (2005).

[2] M. Dijkstra, R. van Roij, and R. Evans, Phys. Rev. E **59**, 5744 (1999).

[3] (a) J. F. Joanny, L. Leibler, and P. G. de Gennes, J. Polym. Sci., Polym. Phys. Ed. **17**, 1073 (1979); (b) J. M. H. M. Scheutjens and G. J. Fleer, Adv. Colloid Interface Sci. **16**, 361 (1982); (c) E. Eisenriegler, J. Chem. Phys. **113**, 5091 (2000); (d) S. Zhou, Chem. Phys. Lett. **392**, 110 (2004); (e) L. Li, D. Bedrov, and G. D. Smith, J. Chem. Phys. **123**, 204504 (2005); (f) D. Léger and D. Levesque, J. Chem. Phys. **123**, 124910 (2005); (g) M. Surve, V. Pryamitsyn, and V. Ganesan, J. Chem. Phys. **122**, 154901 (2005); (h) L. Li, L. Harnau, S. Rosenfeldt, and M. Ballauff, Phys. Rev. E **72**, 051504 (2005).

[4] M. Fuchs and K. S. Schweizer, Phys. Rev. E **64**, 021514 (2001); P. González-Mozuelos, J. M. Méndez-Alcaraz, and R. C. eda-Priego, J. Chem. Phys. **123**, 214907 (2005); H. Freedman and T. N. Truong, J. Phys. Chem. B **109**, 4726 (2005).

[5] D. Chandler and H. C. Anderson, J. Chem. Phys. **57**, 1930 (1972); D. Chandler, *ibid.* **59**, 2742 (1973).

[6] J. G. Curro and K. S. Schweizer, J. Chem. Phys. **87**, 1842 (1987); K. S. Schweizer and J. G. Curro, Adv. Chem. Phys. **98**, 1 (1997), and references therein.

[7] M. Fuchs and K. S. Schweizer, Europhys. Lett. **51**, 621 (2000); J. Phys.: Condens. Matter **14**, R239 (2002); A. Shah, S. Ramakrishnan, Y. L. Chen, K. S. Schweizer, and C. F. Zukoski, *ibid.* **15**, 4751 (2003).

[8] R. Tuinier, H. N. W. Lekkerkerker, and D. G. A. L. Aarts, Phys. Rev. E **65**, 060801(R) (2002).

[9] P. Attard, J. Chem. Phys. **91**, 3083 (1989).

[10] N. Patel and S. A. Egorov, J. Chem. Phys. **121**, 4987 (2004).

[11] S. Zhou, Chem. Phys. Lett. **399**, 323 (2004).

[12] G. A. Martynov, *Fundamental Theory of Liquids. Method of Distribution Functions* (Bristol, Adam Hilger, 1992).

[13] S. Zhou, J. Colloid Interface Sci. **298**, 31 (2006).

[14] S. Zhou, Phys. Lett. A **319**, 279 (2003).

[15] A. Yethiraj and K. S. Schweizer, J. Chem. Phys. **97**, 1455 (1992).

[16] K. G. Honnell, J. G. Curro, and K. S. Schweizer, Macromolecules **23**, 3496 (1990).

[17] S. Zhou, J. Colloid Interface Sci. **288**, 308 (2005).

[18] S. Labik, A. Malijevsky, and P. Vonka, Mol. Phys. **56**, 709 (1985).

[19] F. A. Escobedo and J. J. de. Pablo, J. Chem. Phys. **103**, 1946 (1995).

[20] A. Striolo, C. M. Colina, K. E. Gubbins, N. Elvassore, and L. Lue, Mol. Simul. **30**, 437 (2004).

[21] G. A. Vilegenthart and H. N. W. Lekkerkerker, J. Chem. Phys. **112**, 5364 (2000).

[22] P. Attard, D. R. Berard, C. P. Ursenbach, and G. N. Patey, Phys. Rev. A **44**, 8224 (1991).

[23] A. Yethiraj and C. K. Hall, J. Chem. Phys. **95**, 3749 (1991).

[24] S. Zhou, Chem. Phys. Lett. **399**, 315 (2004).

[25] S. Asakura and F. Oosawa, J. Chem. Phys. **22**, 1255 (1954); A. Vrij, Pure Appl. Chem. **48**, 471 (1976).

[26] A. P. Alivisatos, J. Phys. Chem. **100**, 13226 (1996); L. Li, D. Bedrov, and G. D. Smith, Phys. Rev. E **71**, 011502 (2005).

[27] E. Velasco, G. Navascues, and L. Mederos, Phys. Rev. E **60**, 3158 (1999).

[28] A. Daanoun, C. F. Tejero, and M. Baus, Phys. Rev. E **50**, 2913 (1994).

[29] M. H. J. Hagen and D. Frenkel, J. Chem. Phys. **101**, 4093 (1994).

[30] S. P. Das, Rev. Mod. Phys. **76**, 785 (2004).

[31] J. M. Ortega and W. C. Rheinboldt, *Iterative Solution of Nonlinear Equations in Several Variables* (Academic Press, New York, 1970), Chap. 7.

[32] A. A. Broyles, J. Chem. Phys. **33**, 456 (1960).

[33] W. H. Press, B. P. Flannery, S. A. Teukolsky, and W. T. Vetterling, *Numerical Recipes* (Cambridge University, New York, 1986).

[34] C. Broyden, Math. Comput. **19**, 577 (1965); Comput. J. **12**, 95 (1969).